International Journal of Thermal Sciences 170 (2021) 107172

Contents lists available at ScienceDirect

International Journal of Thermal Sciences

journal homepage: www.elsevier.com/locate/ijts

Colored radiative cooling: How to balance color display and radiative cooling performance

Wang Xi, Yida Liu, Weixian Zhao, Run Hu *, Xiaobing Luo

State Key Laboratory of Coal Combustion, School of Energy and Power Engineering, Huazhong University of Science and Technology, Wuhan, 430074, China

ARTICLE INFO

Keywords:
Radiative cooling
Structural color
Photonic crystal
Metal-dielectric-metal
Selective radiator

ABSTRACT

Radiative cooling, which aims at cooling objects by radiating heat into the outer space through the atmosphere window, has garnered wide interests since it is a passive refrigeration mode without extra energy consumption. However, most of the proposed structures, to maximize the cooling performance, are in white color, which may limit their practical applications due to some aesthetic consideration. To reveal the competing role between color display and radiative cooling performance, we take a metal-dielectric-metal (MDM) colored radiative cooler structure as representative to explore how the structure parameters influence the cooling performance and color display respectively, and clarify the key parameters for the desired performance. Moreover, the reflectance of the colored radiative cooler is identified as peak- and valley-types to clarify the color display performance. The Spearman rank order correlation coefficients between radiative cooling performance and the CIE-LCH color space parameters (lightness, chroma, and hue) are calculated, revealing that the lightness plays a dominant role. The present study is expected to reveal the competing role of radiative cooling power and color display, and trigger the practical applications of radiative cooling technologies.

1. Introduction

Radiative cooling, which aims at radiating heat directly into the sky at ~3 K through the atmosphere windows, has garnered increasing attentions due to zero-energy input, great cooling potential, and widespread applications [1]. Taking the extremely low-temperature outer space as the cold source, objects on the earth at ~300 K can theoretically radiate heat at huge amount according to the Stefan-Boltzmann law. Although this working principle has been proposed for about 60 years, early radiative cooling technologies only works at nighttime for the reason that the solar energy input will easily compensate the cooling power in the daytime. Note that the typical solar intensity is around 1000 W/m^2, while the radiative cooling power is around 100 W/m^2. Even though, early nighttime experiments had demonstrated that a surface could be cooled below the ambient temperature by 10–15 °C, which fuel the subsequent researchers with confidence to explore the daytime radiative cooling technologies [2]. The daytime radiative cooling remains to be a grand challenge, but researchers have been sparing no effort to explore the possible materials and structures to maximize the reflectance in the solar spectrum (0.3–2.5 μm) and emissivity at the atmosphere window (8–13 μm) simultaneously. It is until recent decade that daytime radiative cooling technologies made a great breakthrough thanks to the advance of thermal photonic designs and micro/nano-fabrication techniques. In the first seminal demonstration of daytime radiative cooling, a photonic solar reflector and a thermal emitter was fabricated, which reflects 97% of incident sunlight and exhibits selective emissivity at the atmosphere window simultaneously, and cool to 4.9 °C below the ambient temperature [3]. Later on, many approaches have been proposed for daytime radiative cooling ranging from photonic design, particle-based matrix, composite, textile, etc [4–9]. As for practical applications, these radiative cooling structures, films, and coatings are usually mounted externally for better radiative heat transfer and higher cooling power. However, a new problem arises that the radiative cooler always appears in white color so as to reflect the incident solar light as much as possible, but white colors are not always welcome in some scenarios for the aesthetic reasons. Therefore, the colored radiative cooler (CRC) is more demanded with more practical and broader applications.

To achieve CRC, two strategies were proposed basically [10]. The first one is the dye rendering strategy, which directly applies dye materials onto the surface of the traditional cooler. For example, Chen et al. combined a layer of commercial paints with a porous P(VDF-HFP) or

* Corresponding author.
E-mail address: hurun@hust.edu.cn (R. Hu).

https://doi.org/10.1016/j.ijthermalsci.2021.107172
Received 7 May 2021; Received in revised form 5 July 2021; Accepted 7 July 2021

titanium dioxide (TiO_2)/polymer composite membrane to demonstrate paintable bilayer coatings [11]. Although this strategy can be applied in flexible materials like coating and fabric, the superlayer dye will absorb not only the radiation energy caused by color display in visible band, but also part of radiation energy in infrared band, which will greatly weaken the cooling performance. The second strategy is structural color strategy, which enables color decoration of the cooler through structural design [12–14]. In principle, an object's color can be calculated by the incident radiation spectrum, the reflectance of the object in visible band, and the color matching function of human eye. These three factors represent the process of light projected onto the surface of object, light reflected into human's eyes by the surface, and optical signal converted to electrical signal by human's cones. While the radiation spectrum of sunlight and the color matching function of human eye are fixed and untunable, only through altering visible reflectance of object can one manipulate the color display. Based on this principle, the CRC is realized by designing specific visible reflectance which is based on multi-band emissivity regulation. Compared to the dye rendering strategy, structural color strategy with a complicated and subtle structure can be designed elaborately to avoid extra energy absorbed in infrared waveband, thus enabling better cooling performance. However, it yet suffers from complicated structure design, difficulty and cost in manufacture as well as poor ductility. Lee et al. designed a multi-layer CRC which is the first one based on photonic structure to achieve a good color for CRC with yellow, cyan and magenta colors. When convective heat transfer coefficient $h = 6$ W/(m^2·K), the cooler could get a 3.9 °C lower temperature than the ambient temperature on average [15]. Sheng et al. presented a CRC with no angular dependence by adopting optical Tamm resonance, which got a better cooling effect of 5–6 °C below ambient when $h = 6$ W/(m^2·K) [16]. Li et al. predicted the theoretic limit temperature of radiative cooling and heating corresponding to several kinds of colors and carried out a pink CRC and heater. However, it still lacked practical structures for other colors, and the theoretical potentials of cooling power for CRC remain unsolved [17].

Here, we take a metal-dielectric-metal (MDM) [18,19] colored radiative cooler structure as representative to explore how the structural parameters influence the cooling performance and color display respectively. Different roles of the parameters in color display module are identified through compressive parameter exploration. Moreover, the reflectance spectra of the CRC are categorized into peak- and valley-types, whose characteristics are analyzed thoroughly. Angle dependency of color exhibited by the proposed structure is also studied. Finally, the correlations between radiative cooling power and CIE-LCH color space parameters (lightness, chroma, and hue) are also calculated to offer an intuitional relation between color display and radiative cooling performance.

2. Method

2.1. Cooling power characterization

To quantify the radiative cooling performance, some simplifications are made to simulate the real situation. It should be noted that the radiative cooling effect can be influenced by some environmental conditions such as humidity and clouds, which are not the focus of our discussion. Therefore, the complex practical conditions are simplified to a standard sunny and breezy environment to highlight the focus of our research and make it feasible. With such setup, the cooling power can be denoted by

$$P_{\mathrm{cool}}(T) = P_{\mathrm{rad}}(T) - P_{\mathrm{atm}}(T_{\mathrm{amb}}) - P_{\mathrm{sun}}(\theta) - P_{\mathrm{cond+conv}} \tag{1}$$

where P_{rad} is the output power from the cooler, P_{atm} is the input power from the atmosphere, P_{sun} is the input power from the sun, and the power exchange between the cooler and the environment by conduction and convection is denoted by $P_{\mathrm{cond\ +\ conv}}$. T and T_{amb} are the cooler temperature and the ambient temperature, respectively. θ is angle of solar radiation. Following Ref. [2], the output power from the cooler can be calculated by

$$P_{rad}(T) = \int d\Omega \int_0^{\infty} I_{BB}(T,\lambda)\varepsilon(\lambda,\theta)\cos\theta d\lambda \tag{2}$$

where $\int d\Omega = \int_0^{\pi/2} d\theta \sin\theta \int_0^{2\pi} d\varphi$ is the angular integral over a hemisphere. $I_{\mathrm{BB}}(T, \lambda)$ is the spectral radiance of a blackbody at temperature T and λ is the wavelength [20]. $\varepsilon(\lambda, \theta)$ is the emissivity of the CRC, which is calculated by the transfer matrix method depending on the CRC structure. Similarly, the input power density of the atmospheric radiation absorbed by the cooler is given by

$$P_{atm}(T_{amb}) = \int d\Omega \int_0^{\infty} I_{BB}(T_{amb},\lambda)\varepsilon(\lambda,\theta)\varepsilon_{atm}(\lambda,\theta)\cos(\theta)d\lambda \tag{3}$$

where $\varepsilon_{\mathrm{atm}}(\lambda,\theta) = 1 - \tau(\lambda)^{1/\cos\theta}$ is the emissivity of the atmosphere, and here, $\tau(\lambda)$ is the atmospheric transmittance in the zenith direction [21]. The input solar energy is

$$P_{solar}(\theta) = G\int_0^{\infty} \varepsilon(\lambda,\theta)I_{AM1.5}(\lambda)d\lambda \Big/ \int_0^{\infty} I_{AM1.5}(\lambda)d\lambda \tag{4}$$

where $I_{\mathrm{AM1.5}}(\lambda)$ denotes the standard AM 1.5 spectrum of solar radiation, and G is the total solar irradiance at 1 kW/m^2. The power density of the convection heat transfer is

$$P_{cond+conv} = h_c(T_{amb} - T) \tag{5}$$

where h_c combines the non-radiative heat coefficients of conduction and convection. When the structure and the aforementioned environment conditions are fixed, we can obtain an equation controlling the cooler temperature T and the cooling power P_{cool} by integrating these equations. When P_{cool} is set to be zero, the corresponding cooler temperature is denoted as T_s. A lower T_s means that the cooler can maintain a lower temperature when reaching heat equilibrium and consequently indicates a better cooling performance. In following calculations, the conjugate heat transfer coefficient $h_c = 5$ W/(m^2·K) and the ambient temperature is kept at $T_{amb} = 25$ °C to simulate a breeze situation. All the relevant integrals are computed by discretization summation.

2.2. Color display characterization

Generally, the color of an object depends on three factors: the spectral power distribution of the incident illuminant, the reflectivity of the object in visible spectrum, and color matching functions. The first one relies on the environment, such as the sun, the specific light source, etc. Here, we adopt the standard D65 illumination to represent the typical outdoor daytime sunlight environment. The second one can be adjusted by the materials and structures, which is characterized by the transfer matrix method here for the CRC. The last one is the numerical description of the chromatic response of human eye, which were experimentally characterized by CIE (International Committee on illumination)-XYZ color space in 1931. However, the description of color differences of CIE-XYZ color space is slightly different from human eyes. For better description of the color perceived by human eyes, the CIE-LAB and CIE-LCH color spaces are put forward by the nonlinear transformation of CIE-XYZ color space. CIE-LAB color space has three parameters L^*, a^*, and b^*. L^* is used to represent lightness while a^* and b^* are used to represent chromaticity. These parameters can be transformed from the three tristimulus value X, Y, Z in the CIE-XYZ color space numerically as

$$L^* = 116f(Y/Y_0) - 16 \tag{6}$$

$$a* = 500[f(X/X_0) - f(Y/Y_0)] \tag{7}$$

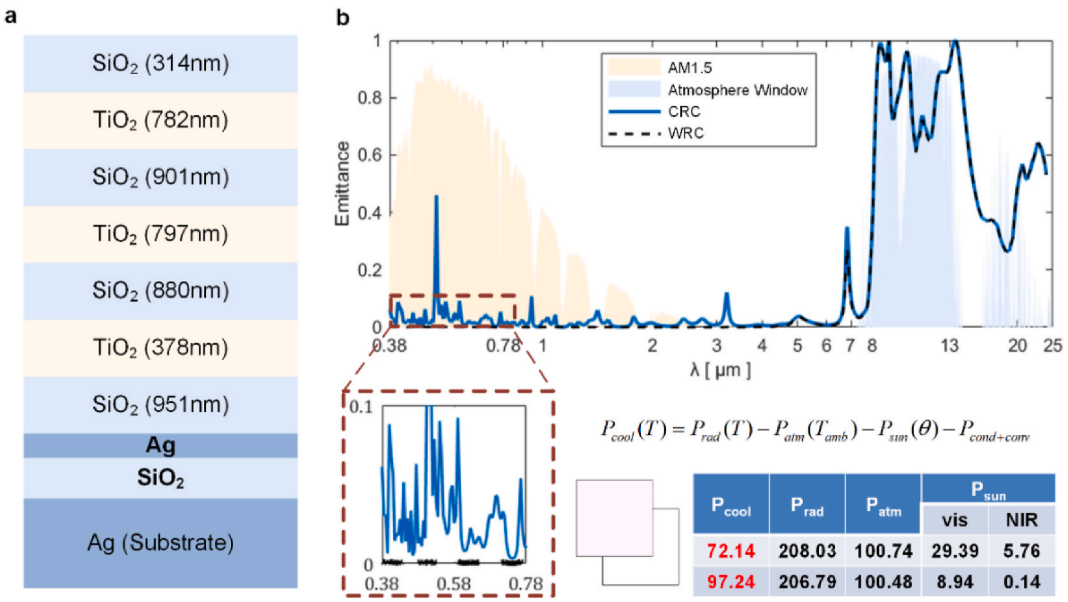

P_{cool}	P_{rad}	P_{atm}	P_{sun}	
			vis	NIR
72.14	208.03	100.74	29.39	5.76
97.24	206.79	100.48	8.94	0.14

Fig. 1. (a) Schematic of a typical CRC, and (b) Emissivity spectra comparison of WRC and CRC and the corresponding detailed power comparation.

$$b* = 200[f(Y/Y_0) - f(Z/Z_0)] \tag{8}$$

where X_0, Y_0, Z_0 are the tristimulus values corresponding to color white, and

$$f(t) = \begin{cases} t^{\frac{1}{3}}, & t > \left(\frac{24}{116}\right)^3 \\ \left(\frac{841}{108}\right)t + \frac{16}{116}, & t \le \left(\frac{24}{116}\right)^3 \end{cases} \tag{9}$$

CIE-LCH color space is just essentially another equivalent form of CIE-LAB color space. It uses lightness ($L = L^*$), chroma ($C = \sqrt{a^{*2} + b^{*2}}$), and hue ($H = \arctan(b^*/a^*)$) to describe colors, which can be expressed by combination of the L^*, a^*, and b^*, respectively. We choose the CIE-LCH color space for it fits better with human visual experience, along with advantages of wider color space and unique color coding.

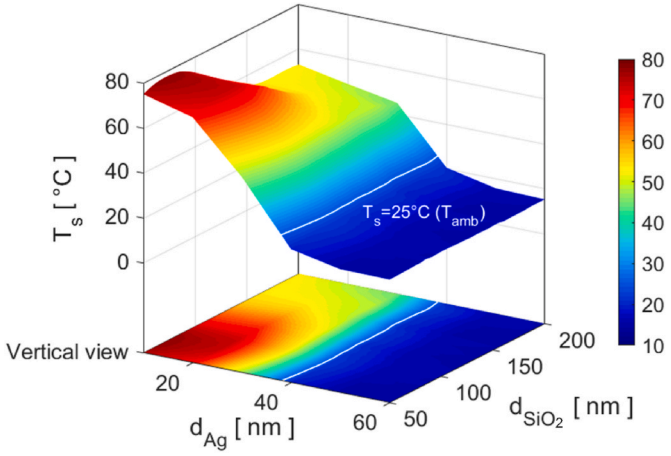

Fig. 2. Steady-state Temperature T_s versus structural parameters.

3. Results and discussion

To simplify the analysis process, we adopt the one-dimensional MDM photonic crystal structures to design the CRC with limited parameters like layer materials, thickness, and configurations. As shown in Fig. 1(a), the CRC can be divided into two parts according to different functionalities, namely the radiative cooling module and color display module. Both the structure and materials are chosen deliberately after a comprehensive review of the existing literature [22–29]. Here, a typical radiative cooling module consists of the SiO_2/TiO_2 photonic crystal with varying layers thickness in Fig. 1(a) while the Ag/SiO_2 layers pair denotes the color display module, whose thicknesses are set to be 50 nm and 125 nm. Without the color display module, the rest structure can be regarded as a conventional white-color radiative cooling module (WRC for short thereinafter). Both the CRC and WRC structures are mounted on a silver substrate for reflection in case. The material properties of TiO_2 are referred from Sarkar's work [23] and Palik's handbook [24], while SiO_2 are referred from Palik's handbook [25]. The optical constants of bulk Ag are referred from Yang's work [26], while optical constants of the thin film Ag come from Kim's work [27]. The emissivity and reflectivity spectra are calculated by transfer matrix method (TMM) [30,31], which is a common lightweight method to solve Maxwell's equations. The emissivity spectra of the WRC and CRC at 0.38–25 μm are shown in Fig. 1(b). It is seen that the emissivity spectra overlap mostly and the only difference occurs in visible spectrum. WRC exhibits near zero emissivity in solar incident band to reflect the input solar radiation energy as much as possible and achieve higher cooling power. Such high reflectance in the visible band generates white color display as a result. In contrast, the CRC exhibits a higher emissivity and a lower reflectivity at ~0.51 μm, thus producing a light-magenta color. Consequently, the absorbed solar radiation energy P_{sun} increases from 9.08 to 35.15 W/m^2, leading to 25.8% reduction of the net radiation cooling power from 97.24 to 72.14 W/m^2. Basically, the increase of the absorbed solar radiation will weaken the radiation cooling power, implying the cooling power and the color display are competing. At thermal equilibrium, the WRC maintains at a low temperature below T_{amb} by 12.76 °C, while the CRC maintains at relatively higher temperature below T_{amb} by 9.44 °C. It should be note that we use a lower steady-state temperature T_s of the CRC to represent a higher cooling power for convenience in this paper. From this preliminary comparison, we note that the main difference between the CRC and WRC lies in the diverse emissivity/reflectivity in the visible band for color display, and the high emissivity (low reflectivity) in the visible band will cause the decrease in cooing power. Therefore, the competing role between the cooling power and the color

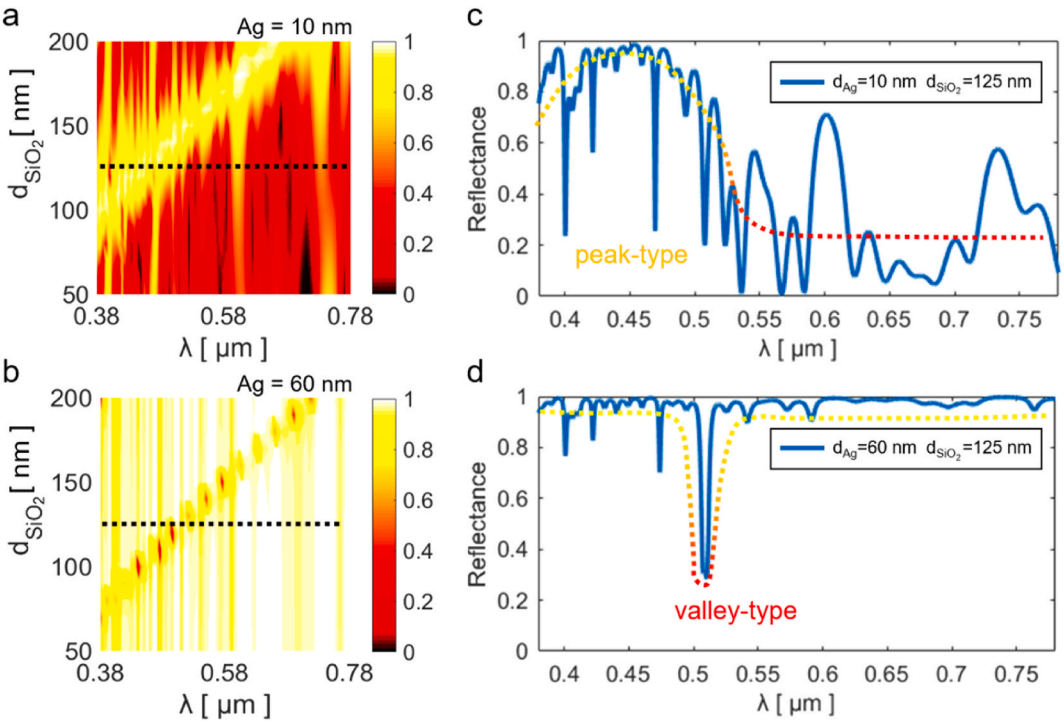

Fig. 3. Reflectance corresponding to different SiO_2 thickness when (a) $d_{Ag} = 10$ nm and (b) 60 nm respectively. (c) Peak-type reflectance when $d_{Ag} = 10$ nm, $d_{SiO2} = 125$ nm; (d) Valley-type reflectance when $d_{Ag} = 60$ nm, $d_{SiO2} = 125$ nm.

display is coupled by the emissivity spectrum. The remaining challenge is how to balance the cooling power and color display by adjusting the structural parameters in the CRC design, and the first step is to reveal how parameters influence on cooling and color.

Fig. 2 shows the variation of CRC steady-state temperature T_s with fixed radiative cooling module and by varying d_{Ag} and d_{SiO2} in the color display module. The white solid line denotes the ambient temperature $T_{amb} = 25\ ^{\circ}C$. The thickness of Ag layer d_{Ag} ranges from 10 nm to 60 nm with a step of 10 nm and the thickness of SiO_2 layer d_{SiO2} ranges from 50 nm to 200 nm with a step of 5 nm. It is seen in Fig. 2 that when the thickness of Ag layer is smaller than 40 nm, the CRC absorbs, rather than radiates, more heat from the ambient, balancing at a rather high steady-state temperature. When the thickness of Ag layer is larger than 40 nm, the CRC tends to show the net cooling effect with a relatively low temperature. Compared to Ag layer thickness, SiO_2 layer thickness is a secondary factor to the cooling effect, which has a limited influence on the cooling power. Therefore, it is advantageous to tune the thickness of Ag layer for better cooling performance.

Although the SiO_2 layer thickness has little influence on the cooling power, it is the major factor for the color display. The reflectance maps, corresponds to the two CRC structures with the same $d_{SiO2} = 125$ nm, and different $d_{Ag} = 10$ nm and 60 nm, are shown in Fig. 3(a–b) respectively. Each horizontal line represents a reflectance spectrum of different d_{SiO2} while color denotes the value of reflectivity. It can be seen that the mean reflectance is low when $d_{Ag} = 10$ nm but near unity when $d_{Ag} = 60$ nm. This indicates that the thicker Ag layer is, the better cooling effect will be, which agrees well with the aforementioned discussion. When altering SiO_2 layer thickness d_{SiO2}, the reflectance can be adjusted according to Fig. 3(a–b), and cause diverse colors. To analyze concretely, Fig. 3(c–d) show the corresponding reflectance spectra of two CRC structures as typical examples with the same $d_{SiO2} = 125$ nm, and different $d_{Ag} = 10$ nm and 60 nm respectively, which matches the black dashed line in Fig. 3(a–b). It is seen that when $d_{Ag} = 10$ nm, the total reflectance is high only between 380 nm and 510 nm. Therefore, the structure will display a superposed color by mixing the light with wavelength between 380 nm and 510 nm. When $d_{Ag} = 60$ nm, the reflectance spectra is high almost at the whole wavelength band except for $\lambda = 510$ nm, which corresponds to the complementary light-magenta color according to additive color-mixing principle. Similar phenomena are also shown with other fixed d_{Ag} as shown in Fig. S1.

From the analysis above, the influence of Ag/SiO_2 layer thicknesses should be discussed in two cases: a thin Ag layer and a thick one. In the first case when $d_{Ag} < 40$ nm, the reflectance in visible band is relatively small except for some reflectivity peaks, which is called as peak-type reflectance. The peak-type reflectance has a low mean reflectance (high absorptance) which leads to more absorbed solar radiation heat and hence a rather poor overall radiative cooling performance. Altering SiO_2 layer thickness can shift the reflectivity peak, and thus influence both the cooling power and color display. For cooling power, as main reflectivity peak deviates from the high energy waveband of the solar radiation spectrum, the input solar radiation P_{sun} will decrease and hence improve the cooling power. Such improvement is weakened with the increase of the Ag layer thickness, corresponding to the situation where steady-state temperature is higher than T_{amb} in Fig. 2. For color display, the main reflectivity peak determines the wavelengths of light reflected from the object and further determines the color of display. In the second case, when $d_{Ag} \geq 40$ nm, the reflectance in visible band is relatively large except for some reflectivity valleys, which is called as valley-type reflectance. The valley-type reflectance makes structure reflect most of the solar radiation outward, leading to a better overall radiation cooling performance. Altering SiO_2 layer thickness can also shift the reflectivity valley and change color display, but the influence on radiative cooling power is neglectable, as shown in Fig. 2. This is because no matter which wavelengths the reflectivity valley lies in, the amount of reflected solar radiation almost maintains the same and hence exhibits little influence on radiative cooling power. When comparing peak-type and valley-type reflectance in visible waveband, it can be concluded that valley-type reflectance with a high mean reflectance is more likely to achieve higher cooling power but suffers from poor color display, while the peak-type reflectance exhibits more kinds of color but with limited cooling power.

To further demonstrate the competing role between radiative cooling

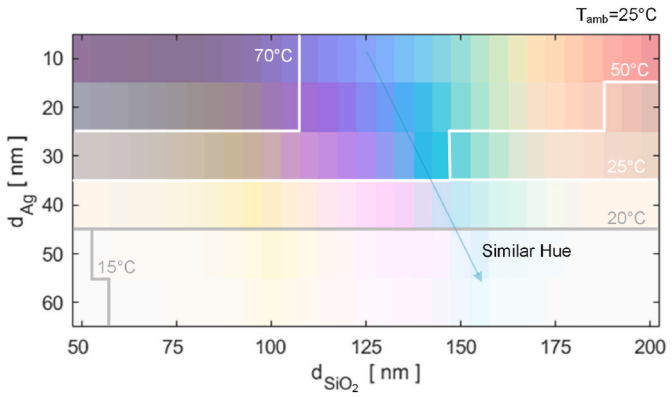

Fig. 4. The color display and the steady-state temperature T_s corresponding to different structural parameters.

and color display and find an intuitive way to gain tradeoff between color display and cooling power, Fig. 4 shows the perceived colors and the corresponding steady-state temperature T_s under different combination of d_{SiO2} and d_{Ag}. In general, large d_{Ag} accounts for higher cooling power while d_{SiO2} accounts for color display, which agrees well with previous analysis. Taking 25 °C as the environmental temperature, the structure with a lower T_s shows limited colors that are rather light and white with poor aesthetics, especially in yellow, magenta and cyan with the reflectivity valley around 450 nm, 500 nm and 620 nm, respectively. On the contrary, more bright and colorful colors can be obtained with a higher T_s, corresponding reduced cooling power. Moreover, as the blue arrow in Fig. 4 indicates, if specific hue of color is desired, a matching of d_{SiO2} and d_{Ag} will fulfill the need. Better color displays with brighter and more vivid colors can be easily achieved by reducing d_{Ag} at the expense of weakening radiative cooling power. Besides, good CRC can also be designed by well designing the color display module with two or even more reflectivity valleys while maintaining acceptable cooling power. For example, the MDM structure with reflectivity valleys at only 450 nm and 620 nm will display green after the superposition of yellow and cyan colors, but still reflect most solar radiation out and keep a good cooling performance. One possible candidate of the color display modules with multiple reflectivity valleys is 2D/3D photonic crystal. Special attention should be paid when combining radiative cooling module and color display module to prevent them from interfering with each other. Besides, there are still some problems such as structure stability to solve for the realization of richer color with cooling effect. What is worth mentioning is the good angular independency of the colors. Fig. 5 demonstrates the reflectance of two structures (d_{Ag} = 10 nm or 40 nm, d_{SiO2} = 125 nm) in different incident angle θ. The corresponding colors under different θ are also shown in the left colorbar. When d_{Ag} = 10 nm in Fig. 5(a), the reflectivity peak still shows up in visible band with a low overall reflectance, leading to the dark tone of color display. The reflectivity peak, which hardly blueshifts when θ increases until θ reaches 40°, starts to shift out of the visible band and cause a lower overall reflectance as well as a darker shade color. Similar trend is also shown in the case of d_{Ag} = 40 nm in Fig. 5(b), except for that the reflectivity valley does not shift out of the visible band, hence leading to the colors with a similar lighter tone under different θ. The consistency of color with little change in range of 0°–40° can avoid information misleading in specific situation such as warning color.

We also quantitatively analyze the correlation between color display and radiative cooling power. Here, the CIE-LCH color space is used to characterize color. As for cooling power, a lower steady-state temperature T_s implies a better cooling performance and a higher cooling power, hence we choose the temperature difference T_{amb}-T_s to represent cooling power for convenience. Fig. 6(a–b) shows the dependence of the three LCH parameters and T_{amb}-T_s on the variation of d_{SiO2}. All parameters are normalized to the same order of magnitude to find out which is the most influential. When d_{Ag} = 10 nm, both the lightness L and T_{amb}-T_s grow gradually with the increase of d_{SiO2}. While d_{Ag} = 40 nm, d_{SiO2} plays a negligible role on these parameters. Moreover, the lightness L has an extremely similar trend with T_{amb}-T_s in both cases. The similar dependences also hold when d_{Ag} < 40 nm and d_{Ag} ≥ 40 nm according to Fig. S2. The spearman rank order correlation coefficients ρ of L, C, H with T_{amb}-T_s are also calculated. The blue points in Fig. 6(c) are approximately aligned linearly with ρ_L = 0.92, which implies a strong linear correlation between lightness L and T_{amb}-T_s. The chroma C is weakly negative correlated with ρ_C = -0.75. This can be seen from Fig. 6 (d) that the smaller chroma C tends to have a better cooling performance. Fig. 6(e) shows well-distributed points with ρ_H = -0.30, which indicated the hue H has almost no correlation with cooling performance. Therefore, color lightness L plays a major role in the competitive relationship between color and cooling effect. Brighter and lighter color stands for better cooling effect, while structures with darker color even fail to maintain cooling effect, which reveals the basic principle for balancing the cooling power and aesthetic needs.

4. Conclusion

In conclusion, we design a CRC with TiO_2/SiO_2 radiative cooler on top of the Ag/SiO_2 color display module to comprehensively investigate the competing role of radiative cooling power and color display. To

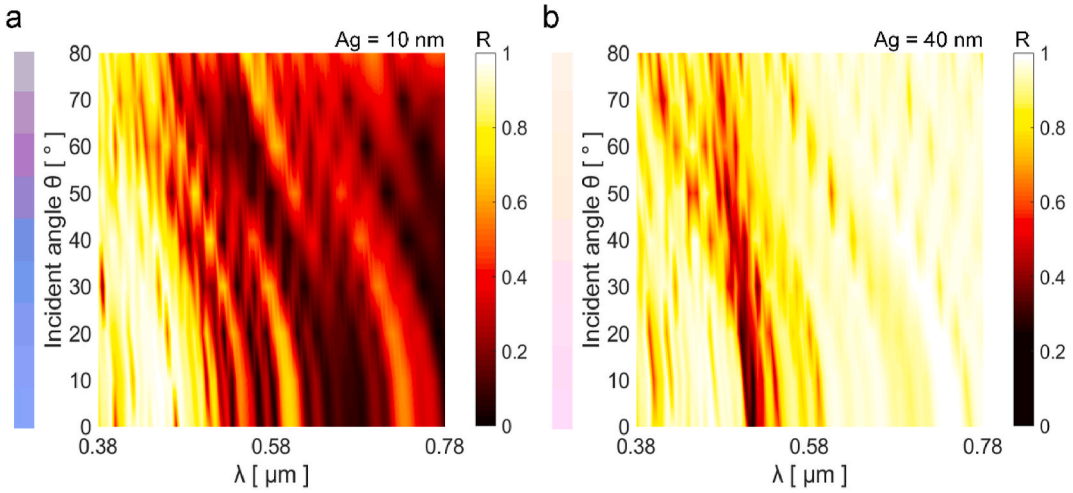

Fig. 5. The angular dependency of reflectance and corresponding color. (a)d_{Ag} = 10 nm, d_{SiO2} = 125 nm (b)d_{Ag} = 40 nm, d_{SiO2} = 125 nm.

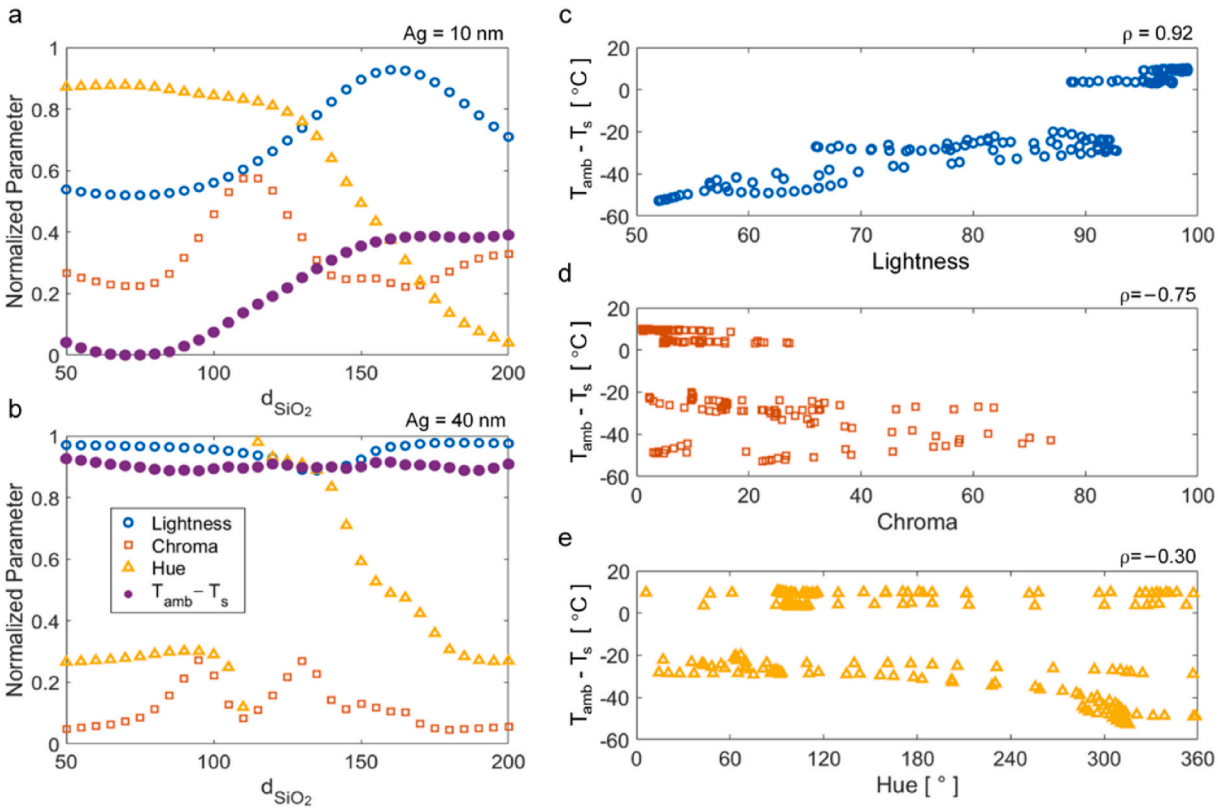

Fig. 6. (a–b) The tendency of the Lightness, Chroma, Hue and T_{amb}-T_s changing with SiO_2 thickness when $d_{Ag} = 10$ nm and 40 nm respectively. (c–e) The spearman rank order correlation coefficients ρ of lightness, chroma, hue with T_{amb}-T_s respectively.

possess a light-magenta color, the CRC, though at the expense of 25.8% net cooling power compared with a WRC, could still maintain a steady-state temperature below the environment temperature by 9.44 °C. The reduced radiative cooling power derives from the additional input solar radiation energy in visible waveband when adding the color display module. Moreover, the parameters of the Ag/SiO_2 color display module play different roles that Ag layer thickness mainly influences radiative cooling power while SiO_2 layer thickness controls color display. The reflectivity spectrum of the CRC could be categorized into peak- and valley-types according to the Ag layer thickness. The valley-type reflectance is more likely to gain a better cooling performance but with limited colors, while the peak-type reflectance tends to have broad kinds of color but with reduced cooling power. Finally, the correlations between radiative cooling power and CIE-LCH color space parameters (lightness, chroma, and hue) are quantitatively analyzed, revealing that the lightness plays a dominant role in the competition between color and radiation cooling. The present study is expected to reveal the competing role of radiative cooling power and color display, highlight the key parameters for the CRC design, and trigger further practical applications of radiative cooling technologies.

Declaration of competing interest

The authors declare that they have no known competing financial interests or personal relationships that could have appeared to influence the work reported in this paper.

Acknowledgment

The authors would like to acknowledge the financial support by National Natural Science Foundation of China (No. 52076087) and the Applied Basic Frontier Programs of Wuhan City (No. 2020010601012197).

Appendix A. Supplementary data

Supplementary data to this article can be found online at https://doi.org/10.1016/j.ijthermalsci.2021.107172.

References

[1] D. Zhao, A. Aili, Y. Zhai, S. Xu, G. Tan, X. Yin, R. Yang, Radiative sky cooling: fundamental principles, materials, and applications, Appl. Phys. Rev. 6 (2) (2019) 21306.
[2] B. Zhao, M.K. Hu, X.Z. Ao, N. Chen, G. Pei, Radiative cooling: a review of fundamentals, materials, applications, and prospects, Appl. Energy 236 (2019) 489–513.
[3] A.P. Raman, M.A. Anoma, L. Zhu, E. Rephaeli, S. Fan, Passive radiative cooling below ambient air temperature under direct sunlight, Nature 515 (7528) (2014) 540–544.
[4] M.A. Kecebas, M.P. Menguc, A. Kosar, K. Sendur, Passive radiative cooling design with broadband optical thin-film filters, J. Quant. Spectrosc. Radiat. Transfer 198 (2017) 179–186.
[5] L. Zhu, A. Raman, K.X. Wang, M.A. Anoma, S. Fan, Radiative cooling of solar cells, Optica 1 (1) (2014) 32–38.
[6] Y. Peng, J. Chen, A.Y. Song, P.B. Catrysse, P.-C. Hsu, L. Cai, B. Liu, Y. Zhu, G. Zhou, D.S. Wu, H.R. Lee, S. Fan, Y. Cui, Nanoporous polyethylene microfibres for large-scale radiative cooling fabric, Nat. Sustain. 1 (2) (2018) 105–112.
[7] P.-C. Hsu, C. Liu, A.Y. Song, Z. Zhang, Y. Peng, J. Xie, K. Liu, C.-L. Wu, P. B. Catrysse, L. Cai, S. Zhai, A. Majumdar, S. Fan, Y. Cui, A dual-mode textile for human body radiative heating and cooling, Sci. Adv. 3 (11) (2017) 1700895.
[8] B. Czapla, A. Srinivasan, Q. Yin, A. Narayanaswamy, Potential for passive radiative cooling by PDMS selective emitters, Proceeding of the ASME Summer Heat Transfer Conference 1 (2017). V001T09A015.
[9] H. Bao, C. Yan, B. Wang, X. Fang, C.Y. Zhao, X. Ruan, Double-layer nanoparticle-based coatings for efficient terrestrial radiative cooling, Sol. Energy Mater. Sol. Cells 168 (2017) 78–84.
[10] M. Srinivasarao, Nano-optics in the biological World: beetles, butterflies, birds, and moths, Chem. Rev. 99 (7) (1999) 1935–1961.
[11] Y. Chen, J. Mandal, W. Li, A. Smith-Washington, C.-C. Tsai, W. Huang, S. Shrestha, N. Yu, R.P.S. Han, A. Cao, Y. Yang, Colored and paintable bilayer coatings with high solar-infrared reflectance for efficient cooling, Sci. Adv. 6 (17) (2020) eaaz5413.
[12] L. Zhu, A. Raman, S. Fan, Color-preserving daytime radiative cooling, Appl. Phys. Lett. 103 (22) (2013) 223902.

[13] R.A. Yalçın, E. Blandre, K. Joulain, J. Drévillon, Colored radiative cooling coatings with nanoparticles, ACS Photonics 7 (5) (2020) 1312–1322.
[14] H.H. Kim, E. Im, S. Lee, Colloidal photonic assemblies for colorful radiative cooling, Langmuir 36 (23) (2020) 6589–6596.
[15] G.J. Lee, Y.J. Kim, H.M. Kim, Y.J. Yoo, Y.M. Song, Colored, Daytime radiative coolers with thin-film resonators for aesthetic purposes, Advanced Optical Materials 6 (22) (2018) 1800707.
[16] C. Sheng, Y. An, J. Du, X. Li, Colored radiative cooler under optical tamm resonance, ACS Photonics 6 (10) (2019) 2545–2552.
[17] W. Li, Y. Shi, Z. Chen, S. Fan, Photonic thermal management of coloured objects, Nat. Commun. 9 (2018) 4240.
[18] H. Shin, M.F. Yanik, S.H. Fan, R. Zia, M.L. Brongersma, Omnidirectional resonance in a metal-dielectric-metal geometry, Appl. Phys. Lett. 84 (22) (2004) 4421–4423.
[19] Q. Li, Z.Z. Li, X.J. Xiang, T.T. Wang, H.G. Yang, X.Y. Wang, Y. Gong, J.S. Gao, Tunable perfect narrow-band Absorber based on a metal-dielectric-metal structure, Coatings 9 (6) (2019) 393.
[20] R. Hu, Y.D. Liu, S. Shin, S.Y. Huang, X.C. Ren, W.C. Shu, J.J. Cheng, G.M. Tao, W. L. Xu, R.K. Chen, X.B. Luo, Emerging materials and strategies for personal thermal management, Adv. Energy Mater. 10 (17) (2020) 1903921.
[21] A. Berk, G. Anderson, P. Acharya, L. Bernstein, L. Muratov, J. Lee, M. Fox, S. Adler-Golden, J. Jr, M. Hoke, R. Lockwood, J. Gardner, Modtran5, update, Proceedings of SPIE - The International Society for Optical Engineering 2006 (2006) 6233.
[22] M.A. Kecebas, M.P. Menguc, A. Kosar, K. Sendur, Spectrally selective filter design for passive radiative cooling, J. Opt. Soc. Am. B 37 (4) (2020) 1173–1182.
[23] S. Sarkar, V. Gupta, M. Kumar, J. Schubert, P.T. Probst, J. Joseph, T.A.F. Konig, Hybridized guided-mode resonances via colloidal plasmonic self-assembled grating, ACS Appl. Mater. Interfaces 11 (14) (2019) 13752–13760.
[24] M.W. Ribarsky, titanium dioxide (TiO2) (rutile), in: E.D. Palik (Ed.), Handbook of Optical Constants of Solids, Academic Press, Burlington, 1997, pp. 795–804.
[25] H.R. Philipp, silicon dioxide (SiO2) (glass), in: E.D. Palik (Ed.), Handbook of Optical Constants of Solids, Academic Press, Burlington, 1997, pp. 749–763.
[26] H.U. Yang, J. D'Archangel, M.L. Sundheimer, E. Tucker, G.D. Boreman, M. B. Raschke, Optical dielectric function of silver, Phys. Rev. B 91 (23) (2015) 235137.
[27] J. Kim, H. Oh, M. Seo, M. Lee, Generation of reflection colors from metal-insulator-metal cavity structure enabled by thickness-dependent refractive indices of metal thin film, ACS Photonics 6 (9) (2019) 2342–2349.
[28] W. Xi, Y.D. Liu, J.L. Song, R. Hu, X.B. Luo, High-throughput screening of a high-Q mid-infrared Tamm emitter by material informatics, Opt. Lett. 46 (4) (2021) 888–891.
[29] J.L. Song, S.Y. Huang, Y.P. Ma, Q. Cheng, R. Hu, X.B. Luo, Radiative metasurface for thermal camouflage, illusion and messaging, Opt Express 28 (2020) 875–885.
[30] C.C. Katsidis, D.I. Siapkas, General transfer-matrix method for optical multilayer systems with coherent, partially coherent, and incoherent interference, Appl. Opt. 41 (19) (2002) 3978–3987.
[31] Z.Y. Li, Principles of the plane-wave transfer-matrix method for photonic crystals, Sci. Technol. Adv. Mater. 6 (7) (2005) 837–841.